Agricultural drought analysis in the Democratic People's Republic of Korea using remote sensing data and GIS technology

GyongBong Ju[1*], YongMin Kim[1], GwangSu Kim[1], YunHui Kim[1]

[1]Hamhung University of Hydraulics and Power, Hamhung 950003, DPR of Korea

[*]Corresponding Author: GyongBong Ju, jkb198922@163.com

Article Info

Keywords:

Agricultural drought, remote sensing data, SPI, VHI, NVSWI, CDI

Abstract:

This paper describes the comprehensive analysis and evaluation of agricultural drought phenomena in the Democratic People's Republic of Korea from 2012 to 2021 using remote sensing technology and GIS technology, which have proven superior in drought research. We analyzed dynamic changes in agricultural drought according to the characteristics of each drought index during the growth period from 2012 to 2021 through the calculation of SPI, VCI, TCI, VHI, and NVSWI derived from time series CHIRPS and MODIS data. The moisture condition index (MCI) was newly proposed starting from the importance of the moisture condition of crops, confirmed reliable by comparing it with the staple agricultural drought indices. Paper proposed a new integrated drought index CDI that comprehensively reflects the vegetation status, soil moisture status, and crop moisture status using the logical calculation function of the geographic information system.

As a result of examining the dynamic change of agricultural drought from 2012 to 2021 using CDI, high temperature and sub-normal rainfall were the main factors causing the drying. The integrated drought index CDI proposed in this paper provides a premise that can be a staple indicator for agricultural drought analysis and evaluation as it is possible to comprehensively and simultaneously consider the vegetation status, soil moisture status, and crop moisture status.

1. Introduction

The character of drought is a lack of precipitation, soil moisture, groundwater, evapotranspiration, and stream flow under average conditions (Anderson et al., 2013, Kumar et al., 2014). Droughts are commonly associated with water shortages due to seasonal rainfall delays and affect people's livelihoods and regional and global economies (Uttaruk & Laosuwan, 2017). Droughts can develop into natural disasters depending on their severity, duration, and frequency, which increases the need for drought monitoring and water resource management systems (Anderson et al., 2011, 2013). Drought is one of the main factors in environmental degradation because it controls the growth of vegetation cover and makes the soil very vulnerable to erosion in the case of concentrated precipitation (Alamdarloo et al., 2018). Therefore, drought monitoring is the most important in providing scientific information for policy establishment and drought risk mitigation (Hua et al., 2019). Droughts can often classify as meteorology, agriculture, hydrology, and socio-economic droughts (Heim, n.d.). Due to the high

temperature and low precipitation, the weather causes meteorological drought due to a lack of water. Due to the meteorological drought, crops are affected by the lack of water, resulting in agricultural drought. Agricultural drought means reduced crop yield due to unreliable rainfall and inadequate soil moisture in the crop root area. (Gidey et al., 2018).

Agricultural drought is difficult to understand because the interaction between vegetation and climate is more complex than other droughts (M. Gao et al., 2008). Traditional methods and point-based datasets alone are not adequate to monitor and evaluate agricultural drought (Du et al., 2018). The relationship analysis between environmental parameters and vegetation cover is a prerequisite for understanding the spatiotemporal changes of agricultural drought for planning and management (Mahajan & Dodamani, 2016). Time-series remote sensing data plays the essential role in detecting, evaluating, and monitoring agricultural drought through real-time data availability and a variety spatial and temporal ranges (Gumma et al., 2019). Multifariousness drought indices have developed to quantify the drought characteristics, particularly severity and spatial extension (Jin & Zhang, 2016). When comparing the remote sensing-based drought index and the field-based drought index, the remote sensing-based drought index is more reliable for monitoring spatiotemporal patterns of drought conditions. The drought index obtained through the time series satellite is very reliable in monitoring and evaluating the drought severity with spatiotemporal resolution in the case of limited observation stations (AghaKouchak et al., 2015). In recent studies, the Climate Hazards Group Infrared Perception with Stations (CHIRPS) dataset was utilized as a substitute for ground-based precipitation data for drought assessment (F. Gao et al., 2018) (Rivera et al., 2019). The Standardized Precipitation Index (SPI) was used as an index for monitoring weather and drought based entirely on precipitation data and as a useful tool (Dutta et al., 2015b) (Quiring & Ganesh, 2010).

(Mckee et al., 1993), SPI provides an easy and flexible way to monitor drought at various scales, from near regularity (-0.99) to extreme drought (<-2.0). Vegetation response depends on environmental factors such as duration, severity, the strength of drought, vegetation phenomena, soil type, agricultural practices, and given location and altitude (Wu et al., 2015;;Dubovyk et al., 2016). Several vegetation indices were studied to monitor the vegetation status in space and time. NDVI (Normalized Difference Vegetation Index) is one of the well-known indices used to monitor and analyze drought occurrence and vegetation health (Berger et al., 2013; Cai et al., 2011; Fan et al., 2018). MODIS provides real-time land surface temperature (LST), and the accessibility of these surface temperature data helps monitor and quantify the correlation between seasonal and interseasonal vegetation dynamics and surface temperature change (Wan, Wang, et al., 2004; Wan, Zhang, et al., 2004). The combination of NDVI and LST provides valuable information and a potent relationship to explain agricultural drought as an early warning system (Zhang et al., 2017). The lack of moisture due to high temperature increases the severity of agricultural drought and directly affects vegetation health. Temperature Condition Index (TCI) and Vegetation Condition Index (VCI) characterize changes in heat and moisture conditions of vegetation, respectively (Bhuiyan et al., 2006; F. N. Kogan, 1995), and the combination of these two indices indicates overall vegetation health. (C. F. Chen et al., 2017). The combination of TCI and VCI has proven to be a practical tool for detecting agricultural drought (Bhuiyan et al., 2006; F. N. Kogan, 2001). The Vegetation Supply Water Index (VSWI) (Carlson et al., 1990a), developed as an agricultural drought index, shows the change in LST for NDVI but has a direct limitation to quantifying the drought severity because of the land cover type and measurement time-sensitivity of the image. Therefore, the normalized VSWI (NVSWI) was proposed (Abbas et al., 2014) and used to measure the severity of the region and the absolute agricultural drought (Abbas et al., 2014; S. Chen et al., 2018a). NVSWI of 0 indicates the most severe drought, and 100 indicates the most humid conditions during the study period. Drought research using remote sensing technology has been conducted extensively in many countries and regions. But there is no case of analyzing long-term fluctuations in drought based on remote sensing using the Democratic People's Republic of Korea as the research area. Therefore, the Monitoring of agricultural drought dynamics in the Democratic People's Republic of Korea was conducted from 2012 to 2021 using various drought indices derived from time-series remote sensing data products in this paper.

This paper has three main contents.

(1) From 2012 to 2021year, the period from June to September, which is the main period for crop growth, was set as the research period, and

then based on MODIS data, NDVI, LST, VCI, TCI, VHI, NDWI (Normalized Difference Water Index) for the study area), MCI, VSWI, and NVSWI to investigate the onset, extent, and intensity of drought.

(2) Based on the calculation of 1-month SPI, 3-month SPI, and 6-month SPI using the CHIRPS (Climate Hazards Group Infrared Precipitation with Stations) dataset, based on correlation analysis with the drought indices calculated above, the agricultural drought in the study area drought index suitable for monitoring determined.

Develop an integrated drought index CDI that comprehensively reflects the characteristics of drought indices by using the logical calculation function of the geographic information system and analyze the agricultural drought dynamics from 2012 to 2021 using the CDI.

2. Materials and Methods

2.1. Research area

The Democratic People's Republic of Korea is located in East Asia (38° to 43° north latitude, 124.5° to 131° east longitude) (Fig 1).

The land area is 123,000 square kilometers, about 80% is mountainous, and about 14% is agricultural land. The annual mean temperature is about 10.7°C, and every twelve months average precipitation is 596.3mm (Park et al., 2017). In summer, it is greatly affected by the East Asian monsoon, and in the rainy season, heavy rains occur (Om et al., 2018). Due to the large annual variability of the East Asian monsoon and the relationship between the intensity and rainfall of the summer monsoon during the rainy season, frequent droughts and floods occur in the study area, causing considerable damage to agricultural activities.

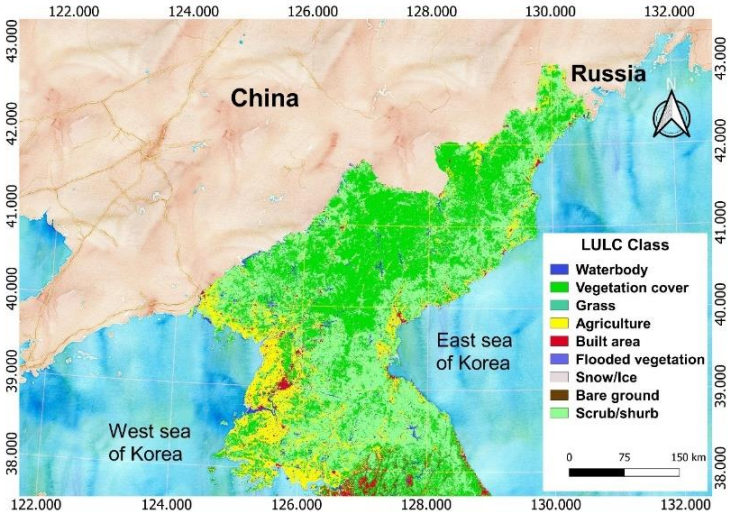

Fig 1. Location map of a research area with land cover grade

2.2. Data collection and preprocessing

2.2.1. Time series CHIRPS data

Nowadays, CHIRPS is an IR-based quasi-global satellite precipitation dataset and is becoming a competent and ideal precipitation dataset for drought monitoring and warning (Funk et al., 2015). CHIRPS has a relatively long-term record (> 30 years) than other satellite precipitation products are developed to support the United States Agency for International Development Famine Early Warning System Network (FEWS NET) and combined through the 'smart' interpolation techniques with an accurate spatial resolution (0.05° × 0.05°). CHIRPS data are available on the website (http://chg.geog.ucsb.edu/data/chirps/). Based on the time series CHIRPS data, monthly precipitation data obtained from 2000 to 2021, and 1-month SPI (1-month SPI), 3-month SPI (3-month SPI), and 6-month SPI (6-month) were calculated.

To maintain the identical resolution as the MODIS data, it interpolated using the raster to point tool and IDW interpolation tool of ArcGIS. Next, the resolution of the SPI raster image increased using the bilinear resampling technique.

2.2.2. Time series MODIS data

The Level-1 and Atmosphere Archive & Distribution System (LAADS) Distributed Active Archive Center (DAAC) website (https://ladsweb.modaps.eosdis.nasa.gov/) with MOD13Q1 data products from 2012 to 2021 MOD11A2 data product was provided. The Terra Moderate Resolution Imaging Spectrum radiometer (MODIS) Vegetation Indices (MOD13Q1) Version 6 data are generated every

16 days at 250 meters (m) spatial resolution as a Level 3 product. The MOD13Q1 product provides two primary vegetation layers. The first is the Normalized Difference Vegetation Index (NDVI) which has referred to as the continuity index to the existing National Oceanic, Atmospheric Administration-Advanced Very High-Resolution Radiometer (NOAA-AVHRR) derived NDVI. The second vegetation layer is the Enhanced Vegetation Index (EVI), which has improved sensitivity over high biomass regions. The algorithm chooses the best available pixel value from all the acquisitions from the 16 days. The criteria used are low clouds, low view angle, and the highest NDVI/EVI value. Along with the vegetation layers and the two quality layers, the HDF file will have MODIS reflectance bands 1 (red), 2 (near-infrared), 3 (blue), and 7 (mid-infrared), as well as four observation layers. The MOD11A2 Version 6 product provides an average 8-day per-pixel Land Surface Temperature and Emissivity (LST&E) with a 1 kilometer (km) spatial resolution in a 1,200 by 1,200 km grid. Each pixel value in the MOD11A2 is a simple average of all the corresponding MOD11A1 LST pixels collected within those eight days. This eight days compositing period was selected because twice of the period is the exact ground track repeat period of the Terra and Aqua platforms. Relevant quality control assessments, hours, monitoring zenith angles of observation, and unclouded sky ranges are allocated with bands 31 and 32 emissivities for land cover types. VCI, TCI, VHI, VSWI, NVSWI, NDWI, and MCI were all calculated using the NDVI of the MOD13Q1 data product and the LST of the MOD11A2. Using the Project Raster tool of ArcGIS, the coordinate system of MODIS products denote as WGS84, WGS84 converted to the WGS84/UTM zone 52N projection system corresponding to the research area. MODIS products are cut out to the boundary of the study area by using ArcGIS' Extract by mask tool and Mosaic tool.

2.3. Method

A flowchart for an overall drought assessment is shown in Fig 2. This process consisted of four steps.

① Using time-series CHIRPS data from 2020 to 2021, calculate 1-month SPI, 3-month SPI, and 6-month SPI in ArcGIS, respectively.

② From 2012 to 2021, MCI, VCI, TCI, VHI, and NVSWI are calculated in ArcGIS using NDVI of MOD13Q1 and LST of MOD11A2, which are time-series MODIS data, respectively.

③ A correlation analysis was progressed with the SPI calculated in ① and the drought indices calculated in (2) to select the drought indices corresponding to the study area and combine them to create an integrated drought index.

④ The comprehensive agricultural drought evaluation of the research area progresses by applying the integrated drought index.

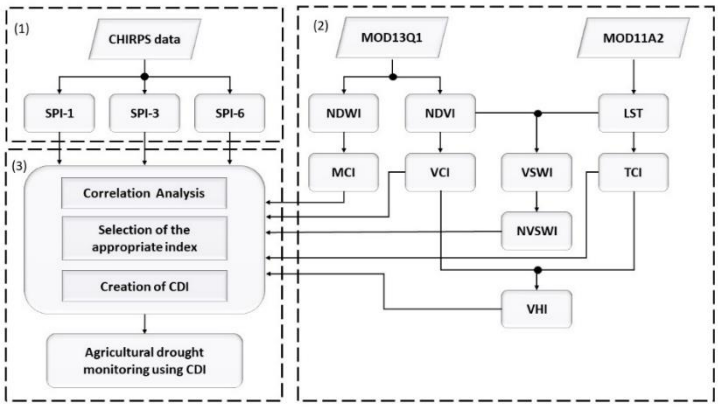

Fig 2. Flowchart for Agricultural Drought Assessment and Monitoring

2.3.1. SPI calculation

(Mckee et al., 1993) designed the SPI to evaluate drought conditions based on the long-term precipitation probability using the gamma function. Precipitation is a normalized value, and SPI is the number of standard deviations from the long-term mean of random variables regularly distributed in the observed precipitation data (Equation (1)). This index provides reliable estimates of the scale and severity of droughts and their spatial extent. If the precipitation is higher than the long-term average, SPI is positive, and if it is low, it means that the SPI is negative. SPI is easy to use because it requires only a single input data series of long-term precipitation compared with other drought indices. Furthermore, since it is based on standardized data, the SPI is spatially invariant and can use to assess drought in other

regions (Guttman, 1998). The Calculation of SPI is as follows.

$$SPI = \frac{X_i - \bar{X}}{\sigma} \quad (1)$$

Where

X_i -Precipitation in the selected period for i years

$\bar{X}$ - Long-term average precipitation

σ - The standard deviation of the selected period

2.3.2. Calculation of Vegetation Condition Index (VCI)

The NDVI-derived VCI has been widely used to detect the onset, intensity, duration, and impact of drought (F. N. Kogan, 1995; Liu & Kogan, 2002; Seiler et al., 1998). The monthly VCI for the growth period from 2012 to 2021 was calculated as follows using the MODIS NDVI (MOD13Q1) dataset in this research.

$$VCI = \frac{(NDVI_i - NDVI_{\min})}{(NDVI_{\max} - NDVI_{\min})} \times 100 \quad (2)$$

$NDVI_i$ -NDVI value of the i th month

$NDVI_{\max}$, $NDVI_{\min}$ - Minimum and maximum values of long-term NDVI values during the study period (2012-2021)

VCI values range from 0 to 100, with a lower value indicating drought and a higher value indicating good vegetation.

2.3.3. Calculation of Temperature Condition Index (TCI)

The design purpose of TCI derived from LST is to evaluate the response stress of plants to water shortage (F. N. Kogan, 1995). This index represents the response of the vegetation cover to the temperature change over time.

The monthly TCI for the growth period from 2012 to 2021 was calculated using the MODIS LST (MOD11A2) dataset in this research.

$$TCI = \frac{(LST_i - LST_{\max})}{(LST_{\max} - LST_{\min})} \times 100 \quad (3)$$

Where

LST_i -LST value of the i th month

$LST_{\min}$, $LST_{\max}$ - Minimum and maximum values of long-term LST values during the study period (2012-2021)

TCI values range from 0 to 100, with a lower value indicating drought and a higher value indicating good vegetation.

2.3.4. Calculation of Vegetation Health Index (VHI)

The Vegetation Health Index (VHI) (F. N. Kogan, 1997, 2001) is necessary agricultural drought indices widely used based on remote sensing information. VHI is composed of a linear combination of the vegetation condition index (VCI), which integrates information on the visible (VIS) and near-infrared (NIR) parts of the electromagnetic spectrum, and the thermal state index (TCI), which depends on the thermal infrared.

The monthly VHI for the growth period from 2012 to 2021 is calculated using VCI and TCI.

$$VHI = \alpha \times VCI + (1-\alpha) \times TCI \quad (4)$$

Here, α is a coefficient that quantifies the relative contribution of moisture and temperature to vegetation health.

2.3.5. Calculation of Normalized Vegetation Supply Water Index (NVSWI)

Vegetation Supply Water Index (VSWI) is one of the widely used indicators of agricultural drought (Carlson et al., 1990b) and shows the relationship between canopy temperature change and soil water supply (S. Chen et al., 2018b). The monthly VSWI for the growth period from 2012 to 2021 was calculated using the NDVI and LST in this research.

$$VSWI = \frac{NDVI}{LST} \quad (5)$$

NVSWI provides a more reasonable drought severity by normalizing the VSWI over a specific time period. The formula for calculating NVSWI is as follows.

$$NVSWI = \frac{(VSWI - VSWI_{\min})}{(VSWI_{\max} - VSWI_{\min})} \times 100 \quad (6)$$

Where

$VSWI$ - Vegetation Supply Water Index for a Specific Period

$VSWI_{\min}$, $VSWI_{\max}$ - Minimum and maximum values of long-term $VSWI$ values during the study period.

The monthly NVSWI for the growth period from 2012 to 2021 was calculated in this research.

2.3.6. Development of Moisture Condition Index (MCI)

The measurement of the moisture content of crops occupies a principal place when analyzing the effects of agricultural drought. NDWI is an indicator to measure the moisture content of leaves and is used to detect and monitor vegetation humidity. NDWI (Normalized Differential Water Index) is an index derived

from NIR and SWIR (Short Wave Infrared) channels, it reflects changes in both the water content (SWIR radiation absorption) and spongy mesophyll of vegetation water pipes (B. Gao, 1996). The NDWI calculated in the 500m SWIR band of MODIS was recently used to detect and monitor the moisture state of the vegetation canopy over a large area (D. Chen et al., 2005; Delbart et al., 2005; JACKSON, 2004; Maki et al., 2004; Xiao et al., 2002). NDWI provides information on the amount of water flowing into plants and can be a more sensitive indicator than NDVI in drought monitoring because it is affected by both dryings and wilting of vegetation crowns (Gu et al., 2007). The Calculation of NDWI is as follows.

$$NDWI = \frac{\rho_{857} - \rho_{2130}}{\rho_{857} + \rho_{2130}} \qquad (7)$$

ρ_{857} and ρ_{2130} are reflectance's at 857 nm and 2130 nm, respectively.

MOD13Q1 product contains 12 layers, of which band2 (16 days Near-Infrared reflectance-841 to 876 nm) and band7 (16 days Middle Infrared reflectance-2105 to 2155 nm) are used to calculate NDWI (Dobri et al., 2021). In this paper, since NDWI can only represent the relative spatial location and cannot compare in time series, MCI (Moisture Condition Index) allows realistic and absolute comparison by normalizing NDWI values within the study period (2012-2021) is a newly proposed.

$$MCI = \frac{\left(NDWI - NDWI_{\min}\right)}{\left(NDWI_{\max} - NDWI_{\min}\right)} \times 100 \qquad (8)$$

Where

$NDWI$ -NDWI is the normalized difference water index for a specific period.

$NDWI_{\min}$ is the minimum value of NDWI pixel during the study period.

$NDWI_{\max}$ is the maximum value of NDWI pixel during the study period.

MCI values range from 0 to 100, with a lower value indicating drought and a higher value indicating wet conditions.

3. Result

The growing season in the study area is from June to September. In the agricultural products of the research area, rice is the main crop. Generally, rice planting in the research area is from May 15 to June 15, and autumn harvesting is from the end of September to the middle of October. In particular, if affected by drought during this growth period, food harvest will decrease, and economic activity will be negatively affected. To analyze the dynamics of agricultural drought in the region during the growth period from 2012 to 2021, SPI and major agricultural drought indices were applied in this research.

3.1. Spatiotemporal dynamics of SPI during three months of the growing season

The three-month SPI compares the total Precipitation from the same 3-month period with the Precipitation in a specific 3-month period for all years included in the historical record. A 3-month SPI reflects short- and medium-term moisture conditions and provides a seasonal estimation of Precipitation. In primary agricultural regions, a 3-month SPI might be more applicable in highlighting available moisture conditions than the slow-responding Palmer Index. Fig 3 shows the spatiotemporal distribution of the 3-month SPI for the study area during the growth period from 2012 to 2021. According to the drought analysis based on Precipitation, droughts above a severe level were observed in 2014, 2019, and June 2017. On the contrary, wet conditions above permit levels were observed in the whole area from July to September 2013, August, September 2020, and June 2021.

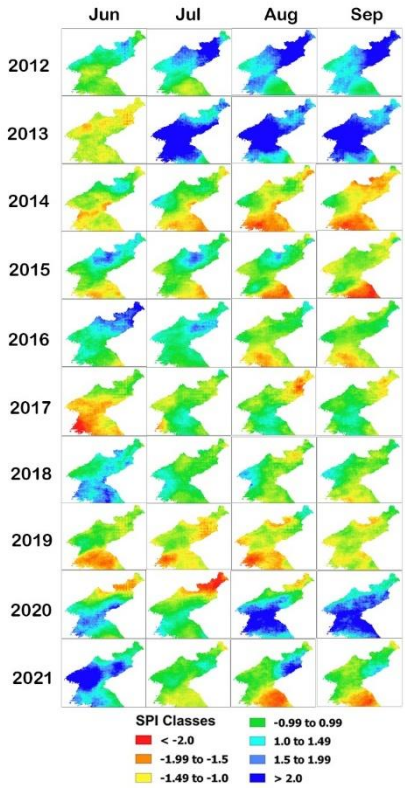

Figure 3

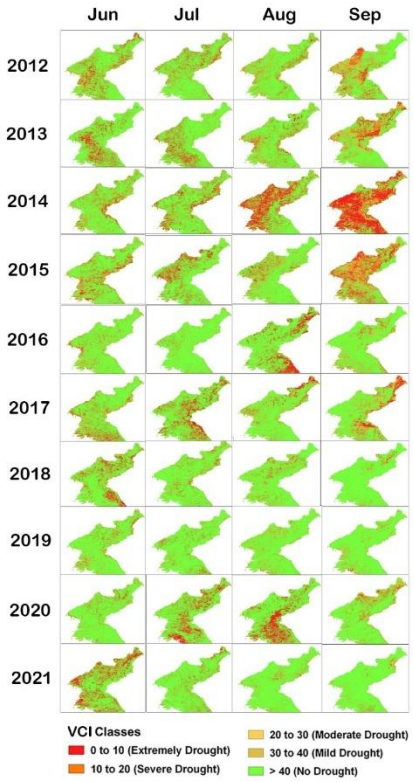

Figure 4

Fig 3. Spatiotemporal distribution of 3-month SPI for study area during the growth period from 2012 to 2021

Fig 4. Spatiotemporal distribution of VCI for research area during the growth period from 2012 to 2021

3.2. VCI's spatiotemporal dynamics

The spatiotemporal distribution of VCI during the growth period from 2012 to 2021 is as follows (Fig 4).

The results of drought analysis based on the vegetation condition are as follows (Table 1).

Table1

Drought analysis result based on vegetation condition

Year	Period	Area	Drought level
2012	June	Central areas	Severe drought
	September	Eastern areas	Severe drought
2013	June ~ August	Central areas, Western areas	Severe drought
	September	Central areas, Eastern Mountainous areas	Severe drought
2014, 2015	June ~ August	Eastern areas, Western areas	Severe drought
	September	All areas	Severe drought
2016, 2017		Eastern areas, Northern areas	Severe drought
2018	June	Eastern areas, Northern areas	Severe drought
2020	July, August	Eastern areas	Severe drought
2021	June	Western areas	Severe drought

3.3. TCI's spatiotemporal dynamics

The spatiotemporal distribution of TCI during the growth period from 2012 to 2021 is as follows (Fig 5).

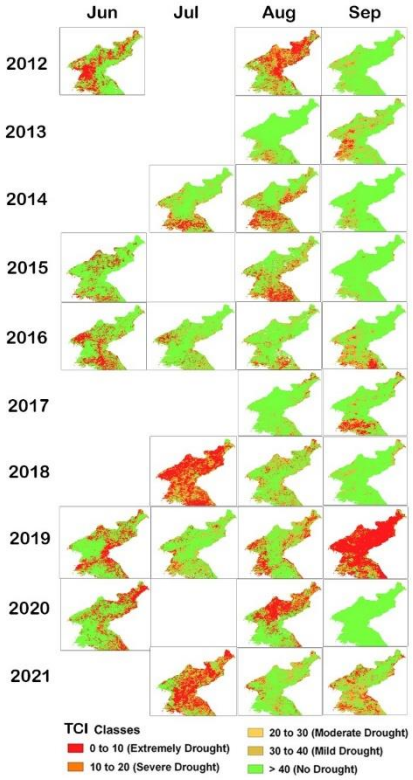

Figure 5

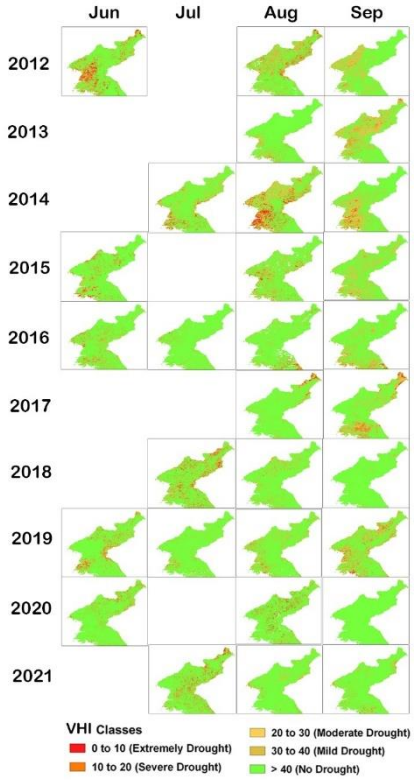

Figure 6

Fig 5. Spatiotemporal distribution of TCI for research area during the growth period from 2012 to 2021

Fig 6. The spatiotemporal distribution of VHI during the growth period from 2012 to 2021

The vacant space in the Fig could not proceed with the drought analysis of some periods due to the severe cloud influence on the LST image. The results of drought analysis according to temperature conditions are as follows (Table 2).

Table 2

Results of drought analysis according to temperature conditions

Year	Period	Area	Drought level
2012	June	Central areas, Western areas	Severe drought
	August	Eastern areas, Northern areas	Severe drought
2013	September	Western areas	Severe drought
2014	July ~ August	Central areas, Eastern areas	Severe drought
2015	August	Western areas, Eastern areas	Severe drought
2016	June	some places in the west and east	Severe drought
2017	September	Central areas	Severe drought
2018	July	All areas	Severe drought
2019	September	All areas	Severe drought
2020	July	All areas	Severe drought

3.4. VHI's spatiotemporal dynamics

The spatiotemporal distribution of VHI during the growth period from 2012 to 2021 is as follows (Fig 6).

The weighted average of VCI and TCI is VHI. The results of drought analysis according to the vegetation condition are as follows (Table 3).

Table 3

Drought analysis results according to vegetation conditions

Year	Period	Area	Drought level
2012	June	Western areas	Severe drought
	August	Eastern areas, Northern areas	Severe drought
	September	Western areas	Severe drought
2013	September	All areas	Severe drought
2014	August	Western areas, Eastern areas	Severe drought
	September	Western areas	Severe drought
2015	September	All areas	Severe drought

2017	September	Central areas	Severe drought
2018	July	Some places in the East and North	Severe drought
2019	June	Some places in the West and East	Severe drought
	September	Western areas, Northern areas	Severe drought
2020	July	All areas	Severe drought

3.5. NVSWI's spatiotemporal dynamics

The spatiotemporal distribution of NVSWI during the growth period from 2012 to 2021 is as follows (Fig 7).

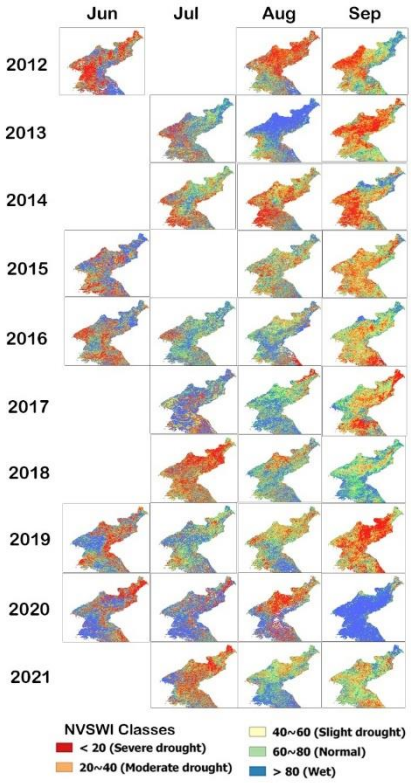

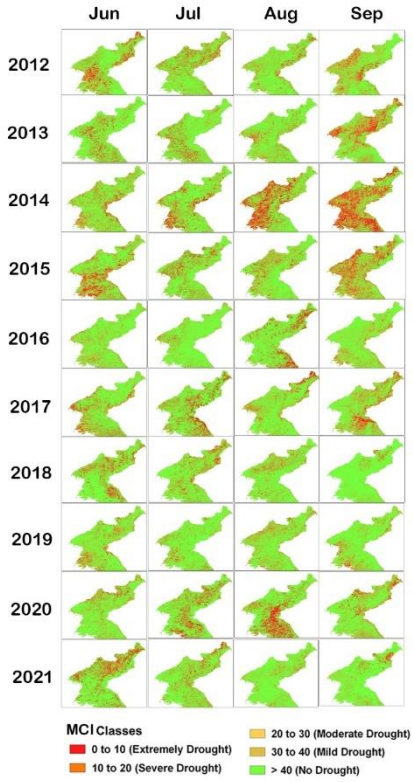

Figure 7 Figure 8

Fig 7. The spatiotemporal distribution of NVSWI during the growth period from 2012 to 2021

Fig 8. The spatiotemporal distribution of MCI during the growth period from 2012 to 2021

According to the results of the drought analysis according to the soil moisture condition, the annual drought period is as follows (Table 4).

Table 4

Duration of drought in each year according to soil moisture conditions

Year	Period	Drought level
2012	June, August, September	Severe drought
2013	September	Severe drought
2014	All periods of growth	Severe drought
2015	All periods of growth	Severe drought
2016	June, September	Severe drought
2017	September	Severe drought
2018	July	Severe drought
2019	All periods of growth	Moderate to severe drought
2020	June, August	Moderate to severe drought
2021	July, August, September	Moderate to severe drought

3.6. MCI's spatiotemporal dynamics

The spatiotemporal distribution of MCI during the growth period from 2012 to 2021 is as follows (Fig 7).

The results of drought analysis according to the moisture state of crops are as follows (Table 5).

Table5
The results of drought analysis according to the moisture state of crops

Year	Period	Area	Drought level
2012	June	Some places in the West and East	Severe drought
	September	Some places in the West and East	Severe drought
2013	September	All areas	Severe drought
2014	August, September	All areas	Severe drought
2015	June	Western areas, Central areas	Severe drought
	September	All areas	Severe drought
2017	September	Central areas	Severe drought
2020	August	Some places in the East	Severe drought
2021	June	Northern areas	Severe drought

3.7. Development of a combined drought index (CDI)

Since MCI, which reflects the moisture state of crops, NVSWI, which express the soil moisture, and VHI, which mirrors the vegetation state, play a fundamental role in agricultural drought evaluation. So it is necessary to consider the three indices simultaneously in space and time by integrating them.

Therefore, this study proposes an integrated drought index that can comprehensively and simultaneously reflect the moisture state of crops, soil moisture state, and vegetation state by using the logical operation function of the geographic information system.

The integrated drought index is as follows.

$$CDI = (MCI \le Dt)\ AND\ (VHI \le Dt)\ AND\ (NVSWI \le Dt) \quad (9)$$

$$\begin{cases} CDI = 1, & Drought \\ CDI = 0, & No\ Drought \end{cases}$$

In Equation (9), Dt is a threshold value that determines the presence or absence of drought.

The values of MCI, NVSWI, and VHI range from 0 to 100.

Many researchers estimate that drought affects crops when the drought index value is less than 40 (Abbas et al., 2014; F. N. Kogan, 1997, 2001). Therefore, in this paper, Dt was determined as 40.

Drought dynamics during the growth period from 2012 to 2021 were analyzed by applying the integrated drought index (Fig 9).

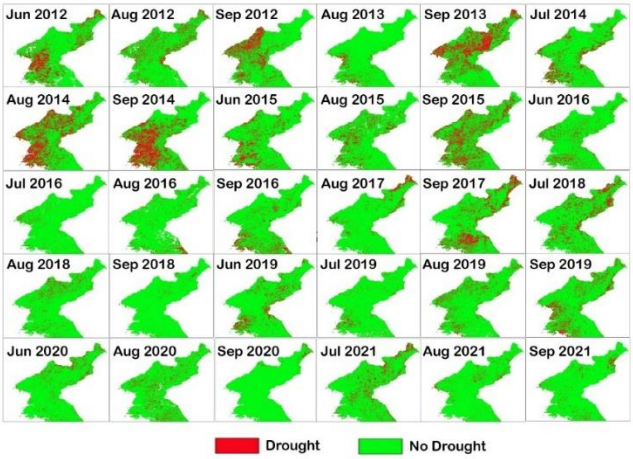

Fig 9. The spatiotemporal distribution of CDI for the research area during the growth period from 2012 to 2021

Table 6 shows the agricultural drought damage situation through the integrated drought index during the growth period from 2012 to 2021.

Table 6
The agricultural drought damage situation through the integrated drought index during the growth period from 2012 to 2021

Date	Agricultural drought area (ha)	Agricultural drought area (%)
Jun 2012	564,289.370	33.63
Aug 2012	224,452.971	13.56
Sep 2012	285,211.350	17.20
Aug 2013	250,094.122	14.82
Sep 2013	401,525.555	24.81
Jul 2014	494,242.470	29.54
Aug 2014	812,527.189	48.34
Sep 2014	740,063.067	43.69
Jun 2015	452,622.051	26.87

Aug 2015	242,661.904	14.41
Sep 2015	519,326.204	31.60
Jun 2016	197,882.793	11.98
Jul 2016	33,259.173	2.14
Aug 2016	47,751.998	2.89
Sep 2016	298,403.536	17.66
Aug 2017	223,709.749	13.89
Sep 2017	514,123.652	30.75
Jul 2018	377,185.043	22.67
Aug 2018	74,322.175	4.63
Sep 2018	6,131.579	0.35
Jun 2019	381,644.373	22.75
Jul 2019	92,531.109	5.51
Aug 2019	197,325.377	11.91
Sep 2019	479,935.451	29.08
Jun 2020	126,347.699	8.04
Aug 2020	48,866.830	2.83
Sep 2020	18,023.127	1.05
Jul 2021	296,173.871	18.18
Aug 2021	80,639.560	4.91
Sep 2021	69,491.234	4.13

As shown in Fig 11 and Table 6, the effects of the drought were severe in 2012, 2014, 2015, 2017, and 2019.

In particular, the drought effect was the most severe in 2014. Fig 10 shows the rainfall status of the study area from 2000 to 2020.

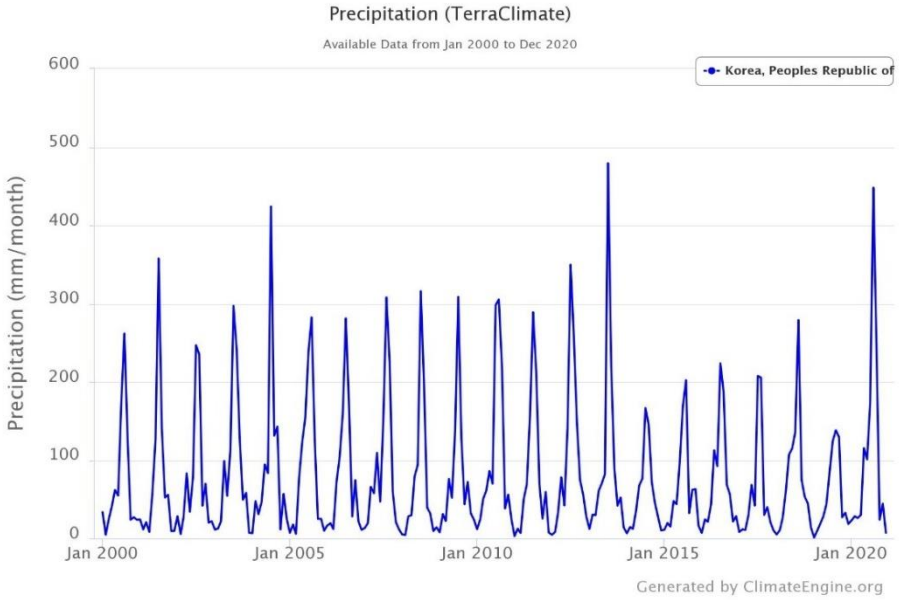

Fig 10. Rainfall status in the study area from 2000 to 2020 (source: http://ClimateEngine.org)

As shown in Fig 10, the rainfall fell sharply from 2014 and recorded low precipitation until 2019. July and August are the rainiest seasons of the year in the study area. However, the average monthly rainfall in July 2014 was 166.4 mm, and in August 2014 was 145.6 mm, the lowest rainfall compared to other years. As shown in Table 6, the area affected by the drought in August 2014 was 812,527.189ha which is 48.34% of the total agricultural land. In fact, in 2014, almost all reservoirs in the study area were depleted, causing significant damage to crops, and the impact continued in 2015.

4. Discussion

4.1. Correlation between SPI and drought indices

Rainfall is a significant factor influencing soil moisture, and the probability of drought occurrence is proportional to the amount of rainfall. In particular, information on the delay time between rainfall and soil moisture implied by the drought index enables more detailed strategies for crop relationships. Therefore, it is necessary to study the relationship between drought and rainfall.

This study used the Pearson correlation coefficient to analyze the correlation between the SPI (1-month SPI, 3-month SPI, 6-month SPI) reflecting the drought condition caused by rainfall and MCI, VHI, and NVSWI, which are major drought indices (Table 7).

Table 7 shows the correlation between SPI and drought indices during the growth period from 2012 to 2021.

Table 7
Correlation between SPI and drought indices during the growth period from 2012 to 2021

Date	SPI	Drought index's				
		MCI	VHI	NVSWI	VCI	TCI
Jun 2012	SPI1	0.038	0.014	-0.080**	0.059	-0.021
	SPI3	0.109**	0.117**	0.026	0.112**	0.070*
	SPI6	0.127**	0.134**	0.040	0.133**	0.076*
Aug 2012	SPI1	0.083*	0.189**	0.258**	0.116**	0.118**
	SPI3	-0.025	-0.263**	-0.352**	-0.021	-0.363**
	SPI6	-0.021	-0.270**	-0.369**	-0.016	-0.379**
Sep 2012	SPI1	0.148**	0.310**	0.255**	0.230**	0.234**
	SPI3	0.146**	0.432**	0.403**	0.307**	0.419**
	SPI6	0.116**	0.384**	0.339**	0.265**	0.382**
Aug 2013	SPI1	0.053	0.157**	0.161**	-0.025	0.305**
	SPI3	-0.037	0.039	0.006	-0.025	0.129**
	SPI6	-0.075*	-0.038	-0.082*	-0.044	0.029
Sep 2013	SPI1	0.135**	0.130**	0.244**	0.214**	-0.069*
	SPI3	-0.138**	-0.176**	-0.185**	-0.043	-0.204**
	SPI6	-0.123**	-0.156**	-0.153**	-0.027	-0.193**
Jul 2014	SPI1	0.033	0.089**	0.076*	0.052	0.138**
	SPI3	0.126**	0.144**	0.109**	0.072*	0.197**
	SPI6	0.123**	0.141**	0.092**	0.087*	0.175**
Aug 2014	SPI1	0.213**	0.217**	0.164**	0.216**	0.035
	SPI3	-0.013	0.011	0.009	-0.173**	0.246**
	SPI6	-0.030	-0.006	0.000	-0.200**	0.254**
Sep 2014	SPI1	-0.143**	-0.190**	-0.278**	-0.109**	-0.171**
	SPI3	-0.133**	-0.079*	-0.235**	-0.168**	0.048
	SPI6	-0.060	0.052	-0.070*	-0.125**	0.195**
Jun 2015	SPI1	0.311**	0.031	0.037	0.190**	-0.117**
	SPI3	0.327**	0.061	0.072	0.207**	-0.082*
	SPI6	0.325**	0.054	0.074*	0.205**	-0.086*
Aug 2015	SPI1	-0.035	0.069	0.154**	-0.078*	0.157**
	SPI3	-0.254**	0.081*	0.009	-0.258**	0.375**
	SPI6	-0.223**	0.123**	0.049	-0.232**	0.391**
Sep 2015	SPI1	0.170**	0.211**	0.217**	0.178**	0.069*
	SPI3	0.003	-0.052	0.027	-0.014	-0.020
	SPI6	0.007	-0.028	0.079*	-0.049	0.133**
Jun 2016	SPI1	0.299**	0.395**	0.371**	0.163**	0.351**
	SPI3	0.198**	0.427**	0.409**	0.112**	0.428**
	SPI6	0.181**	0.425**	0.415**	0.096**	0.441**
Jul 2016	SPI1	0.153**	-0.098*	-0.093*	0.019	-0.224**
	SPI3	0.151**	0.032	0.009	0.065	0.005
	SPI6	0.147**	0.028	0.013	0.044	0.014
Aug 2016	SPI1	-0.072	-0.024	-0.072	-0.018	-0.006
	SPI3	-0.107**	0.008	-0.106**	-0.014	0.024
	SPI6	-0.122**	-0.022	-0.156**	0.033	-0.001
Sep 2016	SPI1	-0.014	0.191**	0.071*	-0.101**	0.390**
	SPI3	0.064	0.214**	0.106**	0.013	0.309**
	SPI6	0.132**	0.315**	0.274**	0.002	0.462**
Aug 2017	SPI1	0.083*	0.374**	0.388**	0.129**	0.418**
	SPI3	0.114**	0.362**	0.421**	0.204**	0.306**
	SPI6	0.099**	0.310**	0.359**	0.181**	0.273**
Sep 2017	SPI1	0.159**	0.281**	0.280**	0.240**	0.195**
	SPI3	0.013	0.086*	0.150**	0.167**	-0.067*
	SPI6	-0.035	0.087*	0.133**	0.118**	-0.012
Jul 2018	SPI1	0.190**	0.047	0.169**	0.079*	-0.087*
	SPI3	0.129**	0.040	0.153**	0.006	-0.021
	SPI6	0.086**	-0.006	0.104**	-0.030	-0.054
Aug 2018	SPI1	-0.136**	-0.185**	-0.176**	-0.019	-0.167**
	SPI3	-0.026	-0.036	0.082**	-0.029	0.001
	SPI6	-0.056	-0.076*	0.009	-0.013	-0.037
Sep 2018	SPI1	-0.081*	-0.250**	-0.224**	-0.019	-0.167**
	SPI3	0.204**	-0.139**	-0.156**	-0.029	0.001

	SPI6	0.173**	-0.120**	-0.119**	-0.013	-0.037
	SPI1	0.093**	0.262**	0.236**	0.102**	0.281**
Jun 2019	SPI3	0.134**	0.316**	0.279**	0.107**	0.327**
	SPI6	0.072*	0.260**	0.228**	0.051	0.305**
	SPI1	0.115**	0.245**	0.235**	0.206**	0.165**
Jul 2019	SPI3	0.164**	0.300**	0.257**	0.189**	0.246**
	SPI6	0.174**	0.289**	0.240**	0.180**	0.227**
	SPI1	-0.022	-0.141**	-0.255**	0.078*	-0.224**
Aug 2019	SPI3	-0.038	-0.135**	-0.212**	0.043	-0.202**
	SPI6	-0.062	-0.170**	-0.248**	-0.001	-0.227**
	SPI1	-0.087**	0.028	0.242**	-0.099**	0.279**
Sep 2019	SPI3	0.012	0.051	0.153**	0.042	-0.040
	SPI6	0.038	-0.005	0.050	0.044	-0.179**
	SPI1	0.146**	0.277**	0.349**	0.000	0.301**
Jun 2020	SPI3	0.144**	0.350**	0.410**	-0.003	0.375**
	SPI6	0.134**	0.283**	0.344**	0.009	0.287**
	SPI1	-0.185**	0.051	0.146**	-0.171**	0.264**
Aug 2020	SPI3	-0.158**	0.248**	0.338**	-0.097**	0.431**
	SPI6	-0.161**	0.252**	0.339**	-0.103**	0.438**
	SPI1	-0.090**	-0.405**	-0.260**	-0.300**	-0.281**
Sep 2020	SPI3	0.105**	0.302**	0.300**	0.216**	0.264**
	SPI6	0.146**	0.373**	0.350**	0.276**	0.325**
	SPI1	-0.157**	0.004	-0.103**	-0.089*	0.096**
Jul 2021	SPI3	-0.050	0.039	-0.033	-0.033	0.074*
	SPI6	-0.028	-0.004	-0.023	-0.058	0.029
	SPI1	-0.185**	-0.250**	-0.295**	-0.260**	-0.115**
Aug 2021	SPI3	-0.197**	-0.304**	-0.355**	-0.254**	-0.169**
	SPI6	-0.171**	-0.268**	-0.298**	-0.258**	-0.134**
	SPI1	-0.056	-0.171**	-0.078*	-0.028	-0.182**
Sep 2021	SPI3	-0.053	0.167**	-0.032	-0.006	0.227**
	SPI6	-0.069*	0.132**	-0.081*	-0.004	0.174**

** Correlation is significant at the 0.01 level (2-tailed).

* Correlation is significant at the 0.05 level (2-tailed).

According to the comprehensive analysis of Table 7, VHI and NVSWI maintained a significant correlation with 3-month SPI, which reflects seasonal precipitation estimates, and shows that the time difference between rainfall and drought is three months. In addition, it provides the premise that VHI and NVSWI can be used as drought indices to characterize drought conditions in the study area.

4.2. Correlation between MCI and major drought indices

In this paper, MCI has newly developed considering the moisture content measurement of crops as a principal indicator in the analysis of agricultural drought. The correlation between MCI and major drought indices was analyzed using the Pearson correlation coefficient to confirm the MCI's usefulness (Table 8).

Table 8

Correlation between MCI and major drought indices

Date	MCI-TCI	MCI-VHI	MCI-NVSWI	MCI-VCI
Jun 2012	0.203**	0.503**	0.292**	0.712**
Aug 2012	0.028	0.299**	0.185**	0.499**
Sep 2012	0.171**	0.513**	0.534**	0.663**
Aug 2013	0.253**	0.465**	0.392**	0.595**
Sep 2013	0.009	0.424**	0.495**	0.652**
Jul 2014	0.216**	0.476**	0.406**	0.618**
Aug 2014	-0.032	0.385**	0.254**	0.642**
Sep 2014	0.275**	0.428**	0.474**	0.544**
Jun 2015	0.097*	0.482**	0.355**	0.720**
Aug 2015	-0.053	0.333**	0.255**	0.592**
Sep 2015	-0.022	0.305**	0.322**	0.507**
Jun 2016	0.061	0.348**	0.228**	0.599**
Jul 2016	-0.012	0.188**	0.200**	0.458**
Aug 2016	0.058	0.242**	0.255**	0.463**
Sep 2016	0.096**	0.327**	0.295**	0.470**
Aug 2017	0.119**	0.412**	0.285**	0.623**
Sep 2017	0.192**	0.431**	0.433**	0.578**
Jul 2018	0.055	0.462**	0.314**	0.678**
Aug 2018	0.029	0.301**	0.259**	0.535**
Sep 2018	-0.093**	0.238**	0.264**	0.506**
Jun 2019	0.085*	0.362**	0.196**	0.610**

Jul 2019	0.094**	0.277**	0.221**	0.417**
Aug 2019	0.051	0.289**	0.205**	0.550**
Sep 2019	-0.128**	0.383**	0.058	0.626**
Jun 2020	0.084*	0.268**	0.147**	0.510**
Aug 2020	-0.079*	0.172**	0.138**	0.505**
Sep 2020	0.162**	0.410**	0.313**	0.577**
Jul 2021	0.137**	0.385**	0.318**	0.621**
Aug 2021	0.133**	0.365**	0.299**	0.569**
Sep 2021	-0.033	0.278**	0.334**	0.556**

** Correlation is significant at the 0.01 level (2-tailed).

* Correlation is significant at the 0.05 level (2-tailed).

Table 8 shows the correlation between MCI and VCI is the biggest. As shown in Fig 10, the rainfall in August 2014 was the lowest at 145.61 mm, and the fall in August 2020 was the highest at 447.98 mm. To further refine the relationship between MCI and major drought indices, extracted scatter plots using data from August 2014 and August 2020 (Fig 11).

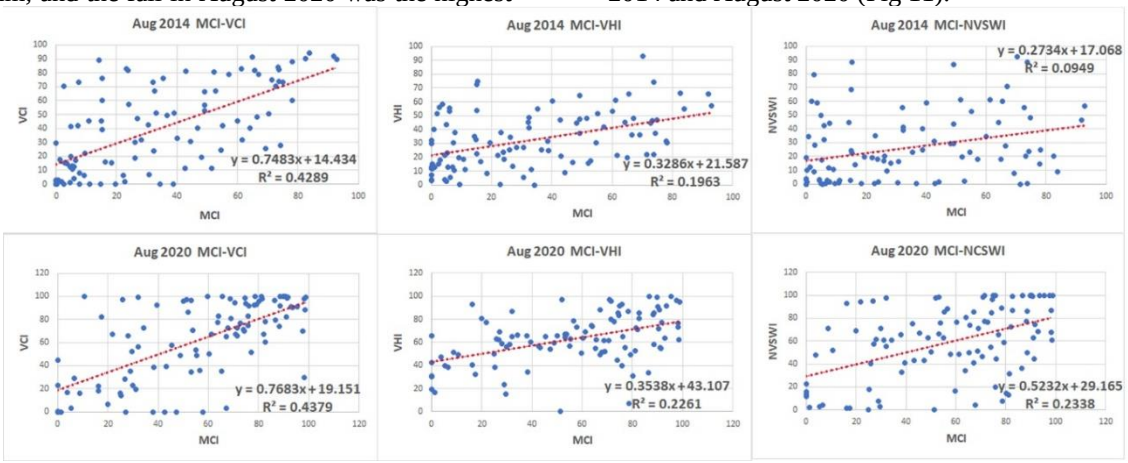

Fig 11. Scatter plot of major drought indices for August 2014 and August 2020 MCI

As can be seen in Fig 11, the correlation between MCI and VCI was the highest. Also, many other studies have recognized VCI as an effective agricultural drought index (Alahacoon & Amarnath, 2022; Arun Kumar et al., 2021; Cao et al., 2022; Dutta et al., 2015a; Wolteji et al., 2022). On the other hand, the fact that MCI and VCI have a high correlation is also the basis for using MCI, which reflects the moisture state of crops, as an agricultural drought index becoming. In addition, the role of MCI must be considered in agricultural drought research for the study area as VHI, which can be said to be the synthesis of VCI and TCI, was selected as the drought index of the study area.

5. Conclusions

We analyzed the first agricultural drought dynamics for the Democratic People's Republic of Korea during the growing period from 2012 to 2021 using various representative drought indices derived from remote sensing data. The spatiotemporal dynamics of rainfall-based drought indices SPI (1-month SPI, 3-month SPI, and 6-month SPI) derived from CHIRPS showed that drought frequently occurred in the entire region from 2014 to 2019. In addition, SPI is used to verify the validity of the agricultural drought index based on the Pearson correlation analysis with the representative agricultural drought indices VCI, TCI, VHI, and NVSWI. As a result, 3-month SPI shows a significant correlation with VHI and NVSWI. Through Spatio-temporal dynamics analysis of VCI, TCI, VHI, and NVSWI, it was possible to analyze the onset, extent, and intensity of drought according to vegetation condition, temperature condition, and soil humidity condition. As a result, in 2012, 2014, 2015, and 2017, it can be seen that the effects of the drought were severe in 2019. In this paper, the moisture condition index MCI was developed starting from the importance of measuring the moisture content of crops in agricultural drought evaluation. In addition, it proved that there is a significant correlation with VCI through correlation analysis between MCI and farming drought indices. We evaluated VHI, NVSWI, and MCI as agricultural drought indices corresponding to the study area through correlation analysis. Also, by using the logical calculation function of the geographic

information system, we proposed a comprehensive drought index CDI that can simultaneously examine the vegetation status, soil moisture status, and crop moisture status. As a result of investigating the spatiotemporal distribution of agricultural drought and the drought-damaged area applying CDI from 2012 to 2021, the worst drought occurred in 2014, and the effect continued in 2015. In addition, the frequency of occurrence of the agricultural drought was higher in the western region than in other zones, and it found that the main factors causing the agricultural dry were relatively high temperature and below-average rainfall. The newly proposed integrated drought index CDI provides a comprehensive and consistent temporal and spatial range of vegetation status, soil moisture status, and crop moisture status, showing its potential as a reliable agricultural drought index in realizing drought mitigation and adaptation strategies.

Acknowledgements

This study was supported by the National Key R&D Program of DPR of Korea (Grant No. 2022RKR927329522) and the Program of Introducing Talents (Grant No. RGC1983117). The authors would like to thank Agency for International Development Famine Early Warning System Network (FEWS NET) for providing CHIRPS data. The authors would like to thank Prof. RI, Hamhung University of Hydraulics and Power, who gave us much valuable advice in the early stages of this work. We also appreciate the editor and anonymous reviewers for their helpful comments.

Disclosure statement

The authors report there are no competing interests to declare

References

Abbas, S., Nichol, J., Qamer, F., & Xu, J. (2014). Characterization of Drought Development through Remote Sensing: A Case Study in Central Yunnan, China. Remote Sensing, 6(6), 4998–5018. https://doi.org/10.3390/rs6064998

AghaKouchak, A., Farahmand, A., Melton, F. S., Teixeira, J., Anderson, M. C., Wardlow, B. D., & Hain, C. R. (2015). Remote sensing of drought: Progress, challenges and opportunities. Reviews of Geophysics, 53(2), 452–480. https://doi.org/10.1002/2014RG000456

Alahacoon, N., & Amarnath, G. (2022). Agricultural drought monitoring in Sri Lanka using multisource satellite data. Advances in Space Research. https://doi.org/10.1016/j.asr.2022.03.009

Alamdarloo, E. H., Manesh, M. B., & Khosravi, H. (2018). Probability assessment of vegetation vulnerability to drought based on remote sensing data. Environmental Monitoring and Assessment, 190(12), 702. https://doi.org/10.1007/s10661-018-7089-1

Anderson, M. C., Hain, C., Otkin, J., Zhan, X., Mo, K., Svoboda, M., Wardlow, B., & Pimstein, A. (2013). An Intercomparison of Drought Indicators Based on Thermal Remote Sensing and NLDAS-2 Simulations with U.S. Drought Monitor Classifications. Journal of Hydrometeorology, 14(4), 1035–1056. https://doi.org/10.1175/JHM-D-12-0140.1

Anderson, M. C., Hain, C., Wardlow, B., Pimstein, A., Mecikalski, J. R., & Kustas, W. P. (2011). Evaluation of Drought Indices Based on Thermal Remote Sensing of Evapotranspiration over the Continental United States. Journal of Climate, 24(8), 2025–2044. https://doi.org/10.1175/2010JCLI3812.1

Arun Kumar, K. C., Reddy, G. P. O., Masilamani, P., Turkar, S. Y., & Sandeep, P. (2021). Integrated drought monitoring index: A tool to monitor agricultural drought by using time-series datasets of space-based earth observation satellites. Advances in Space Research, 67(1), 298–315. https://doi.org/10.1016/j.asr.2020.10.003

Berger, K. A., Wang, Y., & Mather, T. N. (2013). MODIS-derived land surface moisture conditions for monitoring blacklegged tick habitat in southern New England. International Journal of Remote Sensing, 34(1), 73–85. https://doi.org/10.1080/01431161.2012.705447

Bhuiyan, C., Singh, R. P., & Kogan, F. N. (2006). Monitoring drought dynamics in the Aravalli region (India) using different indices based on ground and remote sensing data. International Journal of Applied Earth Observation and Geoinformation, 8(4), 289–302. https://doi.org/10.1016/j.jag.2006.03.002

Cai, G., Du, M., & Liu, Y. (2011). Regional Drought Monitoring and Analyzing Using MODIS Data — A Case Study in Yunnan Province (pp. 243–251). https://doi.org/10.1007/978-3-642-18336-2_29

Cao, S., Zhang, L., He, Y., Zhang, Y., Chen, Y., Yao, S., Yang, W., & Sun, Q. (2022). Effects and contributions of meteorological drought on agricultural drought under different climatic zones and vegetation types in Northwest China. Science of the Total Environment, 821. https://doi.org/10.1016/j.scitotenv.2022.153270

Carlson, T. N., Perry, E. M., & Schmugge, T. J. (1990a). Remote estimation of soil moisture availability and fractional vegetation cover for agricultural fields. Agricultural and Forest Meteorology, 52(1–2), 45–69. https://doi.org/10.1016/0168-1923(90)90100-K

Carlson, T. N., Perry, E. M., & Schmugge, T. J. (1990b). Remote estimation of soil moisture availability and fractional vegetation cover for agricultural fields. Agricultural and Forest Meteorology, 52(1–2), 45–69. https://doi.org/10.1016/0168-1923(90)90100-K

Chen, C. F., Son, N. T., Chen, C. R., Chiang, S. H., Chang, L. Y., & Valdez, M. (2017). Drought monitoring in cultivated areas of Central America using multi-temporal MODIS data. Geomatics, Natural Hazards and Risk, 8(2), 402–417. https://doi.org/10.1080/19475705.2016.1222313

Chen, D., Huang, J., & Jackson, T. J. (2005). Vegetation water content estimation for corn and soybeans using spectral indices derived from MODIS near- and short-wave infrared bands. Remote Sensing of Environment, 98(2–3), 225–236. https://doi.org/10.1016/j.rse.2005.07.008

Chen, S., Muhammad, W., Lee, J.-H., & Kim, T.-W. (2018a). Assessment of Probabilistic Multi-Index Drought Using a Dynamic Naive Bayesian Classifier. Water Resources Management, 32(13), 4359–4374. https://doi.org/10.1007/s11269-018-2062-x

Chen, S., Muhammad, W., Lee, J.-H., & Kim, T.-W. (2018b). Assessment of Probabilistic Multi-Index Drought Using a Dynamic Naive Bayesian Classifier. Water Resources Management, 32(13), 4359–4374. https://doi.org/10.1007/s11269-018-2062-x

Delbart, N., Kergoat, L., le Toan, T., Lhermitte, J., & Picard, G. (2005). Determination of phenological dates in boreal regions using normalized difference water index. Remote Sensing of Environment, 97(1), 26–38. https://doi.org/10.1016/j.rse.2005.03.011

Dobri, R.-V., Sfîcă, L., Amihăesei, V.-A., Apostol, L., & Ţîmpu, S. (2021). Drought Extent and Severity on Arable Lands in Romania Derived from Normalized Difference Drought Index (2001–2020). Remote Sensing, 13(8), 1478. https://doi.org/10.3390/rs13081478

Du, T. L. T., du Bui, D., Nguyen, M. D., & Lee, H. (2018). Satellite-based, multi-indices for evaluation of agricultural droughts in a highly dynamic tropical catchment, Central Vietnam. Water (Switzerland), 10(5). https://doi.org/10.3390/w10050659

Dubovyk, O., Landmann, T., Dietz, A., & Menz, G. (2016). Quantifying the Impacts of Environmental Factors on Vegetation Dynamics over Climatic and Management Gradients of Central Asia. Remote Sensing, 8(7), 600. https://doi.org/10.3390/rs8070600

Dutta, D., Kundu, A., Patel, N. R., Saha, S. K., & Siddiqui, A. R. (2015a). Assessment of agricultural drought in Rajasthan (India) using remote sensing derived Vegetation Condition Index (VCI) and Standardized Precipitation Index (SPI). Egyptian Journal of Remote Sensing and Space Science, 18(1), 53–63. https://doi.org/10.1016/j.ejrs.2015.03.006

Dutta, D., Kundu, A., Patel, N. R., Saha, S. K., & Siddiqui, A. R. (2015b). Assessment of agricultural drought in Rajasthan (India) using remote sensing derived Vegetation Condition Index (VCI) and Standardized Precipitation Index (SPI). The Egyptian Journal of Remote Sensing and Space Science, 18(1), 53–63. https://doi.org/10.1016/j.ejrs.2015.03.006

Fan, X., Liu, Y., Tao, J., Wang, Y., & Zhou, H. (2018). MODIS detection of vegetation changes and investigation of causal factors in Poyang Lake basin, China for 2001–2015. Ecological Indicators, 91, 511–522. https://doi.org/10.1016/j.ecolind.2018.04.041

Funk, C., Peterson, P., Landsfeld, M., Pedreros, D., Verdin, J., Shukla, S., Husak, G., Rowland, J., Harrison, L., Hoell, A., & Michaelsen, J. (2015). The climate hazards infrared precipitation with stations - A new environmental record for monitoring extremes. Scientific Data, 2. https://doi.org/10.1038/sdata.2015.66

Gao, B. (1996). NDWI—A normalized difference water index for remote sensing of vegetation liquid water from space. Remote Sensing of Environment, 58(3), 257–266. https://doi.org/10.1016/S0034-4257(96)00067-3

Gao, F., Zhang, Y., Ren, X., Yao, Y., Hao, Z., & Cai, W. (2018). Evaluation of CHIRPS and its application for drought monitoring over the Haihe River Basin, China. Natural Hazards, 92(1), 155–172. https://doi.org/10.1007/s11069-018-3196-0

Gao, M., Qin, Z., Zhang, H., Lu, L., Zhou, X., & Yang, X. (2008). Remote Sensing of Agro-droughts in Guangdong Province of China Using MODIS Satellite Data. Sensors, 8(8), 4687–4708. https://doi.org/10.3390/s8084687

Gidey, E., Dikinya, O., Sebego, R., Segosebe, E., & Zenebe, A. (2018). Analysis of the long-term agricultural drought onset, cessation, duration, frequency, severity and spatial extent using Vegetation Health Index (VHI) in Raya and its environs, Northern Ethiopia. Environmental Systems Research, 7(1). https://doi.org/10.1186/s40068-018-0115-z

Gu, Y., Brown, J. F., Verdin, J. P., & Wardlow, B. (2007). A five-year analysis of MODIS NDVI and NDWI for grassland drought assessment over the central Great Plains of the United States. Geophysical Research Letters, 34(6), L06407. https://doi.org/10.1029/2006GL029127

Gumma, Nelson, & Yamano. (2019). Mapping drought-induced changes in rice area in India. International Journal of Remote Sensing, 40(21), 8146–8173. https://doi.org/10.1080/01431161.2018.1547456

Guttman, N. B. (1998). COMPARING THE PALMER DROUGHT INDEX AND THE STANDARDIZED PRECIPITATION INDEX. Journal of the American Water Resources Association, 34(1), 113–121. https://doi.org/10.1111/j.1752-1688.1998.tb05964.x

Heim, R. R. (n.d.). A Review of Twentieth-Century Drought Indices Used in the United States.

Hua, L., Wang, H., Sui, H., Wardlow, B., Hayes, M. J., & Wang, J. (2019). Mapping the spatial-temporal dynamics of vegetation response lag to drought in a semi-arid region. Remote Sensing, 11(16). https://doi.org/10.3390/rs11161873

JACKSON, T. (2004). Vegetation water content mapping using Landsat data derived normalized difference water index for corn and soybeans. Remote Sensing of Environment, 92(4), 475–482. https://doi.org/10.1016/j.rse.2003.10.021

Jin, S., & Zhang, T. (2016). Terrestrial Water Storage Anomalies Associated with Drought in Southwestern USA from GPS Observations. Surveys in Geophysics, 37(6), 1139–1156. https://doi.org/10.1007/s10712-016-9385-z

Kogan, F. (2002). World droughts in the new millennium from AVHRR-based vegetation health indices. Eos, Transactions American Geophysical Union, 83(48), 557. https://doi.org/10.1029/2002EO000382

Kogan, F. N. (1995). Application of vegetation index and brightness temperature for drought detection. Advances in Space Research, 15(11), 91–100. https://doi.org/10.1016/0273-1177(95)00079-T

Kogan, F. N. (1997). Global Drought Watch from Space. Bulletin of the American Meteorological Society, 78(4), 621–636. https://doi.org/10.1175/1520-0477(1997)078<0621:GDWFS>2.0.CO;2

Kogan, F. N. (2001). Operational Space Technology for Global Vegetation Assessment. Bulletin of the American Meteorological Society, 82(9), 1949–1964. https://doi.org/10.1175/1520-0477(2001)082<1949:OSTFGV>2.3.CO;2

Kumar, S. v., Peters-Lidard, C. D., Mocko, D., Reichle, R., Liu, Y., Arsenault, K. R., Xia, Y., Ek, M., Riggs, G., Livneh, B., & Cosh, M. (2014). Assimilation of Remotely Sensed Soil Moisture and Snow Depth Retrievals for Drought Estimation. Journal of Hydrometeorology, 15(6), 2446–2469. https://doi.org/10.1175/JHM-D-13-0132.1

Liu, W. T., & Kogan, F. (2002). Monitoring Brazilian soybean production using NOAA/AVHRR based vegetation condition indices. International Journal of Remote Sensing, 23(6), 1161–1179. https://doi.org/10.1080/01431160110076126

Mahajan, D. R., & Dodamani, B. M. (2016). Spatial and temporal drought analysis in the Krishna river basin of Maharashtra, India. Cogent Engineering, 3(1), 1185926. https://doi.org/10.1080/23311916.2016.1185926

Maki, M., Ishiahra, M., & Tamura, M. (2004). Estimation of leaf water status to monitor the risk of forest fires by using remotely sensed data. Remote Sensing of Environment, 90(4), 441–450. https://doi.org/10.1016/j.rse.2004.02.002

Mckee, T. B., Doesken, N. J., & Kleist, J. (1993). THE RELATIONSHIP OF DROUGHT FREQUENCY AND DURATION TO TIME SCALES. In Eighth Conference on Applied Climatology.

Nichol, J. E., & Abbas, S. (2015). Integration of remote sensing datasets for local scale assessment and prediction of drought. Science of The Total Environment, 505, 503–507. https://doi.org/10.1016/j.scitotenv.2014.09.099

Om, K.-C., Ren, G., Li, S., & Kang-Chol, O. (2018). Climatological characteristics and long-term variation of rainy season and torrential rain over DPR Korea. Weather and Climate Extremes, 22, 48–58. https://doi.org/10.1016/j.wace.2018.09.003

Park, S., Im, J., Park, S., & Rhee, J. (2017). Drought monitoring using high resolution soil moisture through multi-sensor satellite data fusion over the Korean peninsula. Agricultural and Forest Meteorology, 237–238, 257–269. https://doi.org/10.1016/j.agrformet.2017.02.022

Quiring, S. M., & Ganesh, S. (2010). Evaluating the utility of the Vegetation Condition Index (VCI) for monitoring meteorological drought in Texas. Agricultural and Forest Meteorology, 150(3), 330–339. https://doi.org/10.1016/j.agrformet.2009.11.015

Rivera, J. A., Hinrichs, S., & Marianetti, G. (2019). Using CHIRPS Dataset to Assess Wet and Dry Conditions along the Semiarid Central-Western Argentina. Advances in Meteorology, 2019, 1–18. https://doi.org/10.1155/2019/8413964

Seiler, R. A., Kogan, F., & Sullivan, J. (1998). AVHRR-based vegetation and temperature condition indices for drought detection in Argentina. Advances in Space Research, 21(3), 481–484. https://doi.org/10.1016/S0273-1177(97)00884-3

Uttaruk, Y., & Laosuwan, T. (2017). Drought Detection by Application of Remote Sensing Technology and Vegetation Phenology. Journal of Ecological Engineering, 18(6), 115–121. https://doi.org/10.12911/22998993/76326

Wan, Z., Wang, P., & Li, X. (2004). Using MODIS Land Surface Temperature and Normalized Difference Vegetation Index products for monitoring drought in the southern Great Plains, USA. International Journal of Remote Sensing, 25(1), 61–72. https://doi.org/10.1080/0143116031000115328

Wan, Z., Zhang, Y., Zhang, Q., & Li, Z.-L. (2004). Quality assessment and validation of the MODIS global land surface temperature. International Journal of Remote Sensing, 25(1), 261–274. https://doi.org/10.1080/0143116031000116417

Wolteji, B. N., Bedhadha, S. T., Gebre, S. L., Alemayehu, E., & Gemeda, D. O. (2022). Multiple Indices Based Agricultural Drought Assessment in the Rift Valley Region of Ethiopia. Environmental Challenges, 7. https://doi.org/10.1016/j.envc.2022.100488

Wu, D., Zhao, X., Liang, S., Zhou, T., Huang, K., Tang, B., & Zhao, W. (2015). Time-lag effects of global vegetation responses to climate change. Global Change Biology, 21(9), 3520–3531. https://doi.org/10.1111/gcb.12945

Xiao, X., Boles, S., Liu, J., Zhuang, D., & Liu, M. (2002). Characterization of forest types in Northeastern China, using multi-temporal SPOT-4 VEGETATION sensor data. Remote Sensing of Environment, 82(2–3), 335–348. https://doi.org/10.1016/S0034-4257(02)00051-2

Zhang, X., Yamaguchi, Y., Li, F., He, B., & Chen, Y. (2017). Assessing the Impacts of the 2009/2010 Drought on Vegetation Indices, Normalized Difference Water Index, and Land Surface Temperature in Southwestern China. Advances in Meteorology, 2017, 1–9. https://doi.org/10.1155/2017/6837493